PERFORMANCE OF TOP-DOWN BASEMENT EXCAVATION FOR THE SINGAPORE ESPLANADE CAR PARK

I. H. Wong[1] and A. T.C. Goh[2]

ABSTRACT: The car park for the Singapore Esplanade is 65 to 109m wide and 184 to 224m long and consists of two levels of basements. The car park was constructed using the top-down method. The performance of the retaining diaphragm walls supporting the excavation are presented in this paper with focus on the lateral wall deflections and the wall bending moments. This paper briefly describes two approaches of deducing bending moments in the diaphragm walls. In addition, back-analyses were also carried out using a finite element program that incorporated the effects of cracking of the wall. The post construction re-analysis indicates that cracking could result in a substantial reduction in the bending moments in the diaphragm wall and a small increase in the lateral wall deflections. Some measurements of the changes in the measured total lateral earth pressures are also presented.

Keywords: bending moments; diaphragm wall; excavation; finite element method; wall deflection.

INTRODUCTION

The Singapore Arts Center, also known as the Esplanade, was completed in 2002. In conjunction with this performing arts complex, a large underground car park, the Esplanade Car Park, was built to accommodate the parking needs of the patrons. The car park is 65 to 109m wide and 184 to 224m long and consists of two levels of basements. The basements were constructed by the top-down method, with excavation depths ranging from 10 to 11.4m below the ground surface and diaphragm walls as retention system. The site, as shown in Fig. 1, is located at Raffles Avenue, next to the Marina Bay and the Singapore River, and comprises thick deposits of soft soils. The south and west wall boundaries were retained by 1.0m thick diaphragm walls while a 0.8m thick wall was adopted for the north wall boundary as the soft soils were thinner there. A temporary composite sheet pile (FSP III) and soldier pile wall was chosen for the east wall boundary that connects the Esplanade Car Park to the Singapore Arts Center. The diaphragm wall lengths were deepest at the south wall boundary, where the combined thickness of the soft soils was largest, with the wall lengths ranging from 33.5 to 35.5m. For the west wall boundary, the wall lengths ranged from 20.7 to 34.0m, with wall lengths decreasing from the south towards the north wall boundary. The wall lengths for the north wall boundary ranged from 23.5 to 28.5m.

The top-down method of basement construction was chosen as part of the roof of the car park was required to be open to traffic for the road extension of the adjacent Nicoll Highway, prior to the completion of the entire basement. The use of diaphragm walls facilitated the top-down method of basement construction. The diaphragm walls also provided maximum economy as the walls served as both temporary and permanent ground supports.

In the first part of this paper, two approaches of deducing bending moments in the diaphragm walls are discussed and the performance of three instrumented diaphragm wall panels is presented with focus on the lateral wall deflections and the wall bending moments.

In the second part of this paper, the results of post construction re-analysis using a modified version of the finite element program EXCAV (Duncan and Chang 1977) considering the effects of cracking of the wall are presented.

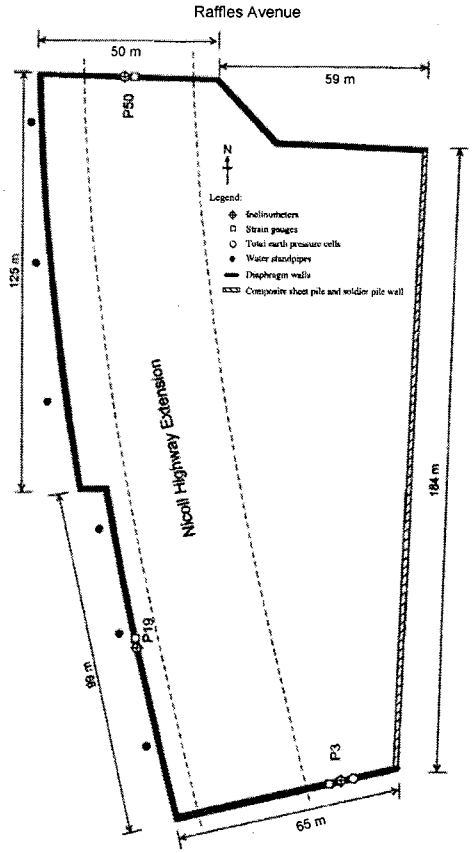

Fig. 1 Plan layout of basement excavation for the Esplanade Car Park

DETERMINATION OF BENDING MOMENTS IN DIAPHRAGM WALLS

In this project, both strain gauges and in-wall inclinometers were used to deduce the bending moments in the diaphragm walls. A brief description is given herein.

[1] Principal Consultant, Mitic Assoc., 336 River Valley Road, No.08-03, Singapore 238366. (Corresponding author: email: inghwong@singnet.com.sg)

[2] Associate Professor, School of Civil and Environmental Engineering, Nanyang Technological University, Singapore 639798

Mathematical details of how the bending moments can be derived from these two methods are presented in the Poh et al. (1997). The wall bending moment is defined herein as positive when the tension face of the wall is on the excavation side.

Bending moments along a diaphragm wall can be obtained by knowing the material and sectional properties, and the curvature along the wall section. The commonly accepted method of measuring wall curvatures, and hence the bending moments of a diaphragm wall, is by installing vibrating wire strain gauges in the diaphragm wall. This method of measurement only provides curvatures at the points where the strain gauges are located. The strain gauges need to be installed at close intervals in order to have a more comprehensive profile of bending moments along the wall section, thereby requiring a large number of strain gauges. Since this is often not economically feasible, in practice, the strain gauges are only installed at wall locations where large bending moments are expected. As a strain gauge is an electrical device, it is sensitive to external loads. The strain gauges may also be damaged or malfunction during the lowering of the steel reinforcement cage into the slurry trench, or during the concreting of the diaphragm wall. In practice, strain gauges are generally installed at 2 to 3m intervals in the zone of interest. If some of the strain gauges are damaged during the construction of the wall panel, then there will be no measurements of bending moments for a large section of the wall.

An alternative method of obtaining wall curvatures is by installing an inclinometer inside the diaphragm wall during the construction of the wall panel. Inclinometers are commonly used in projects involving propped excavations as they are one of the basic instruments required for construction control. Inclinometers installed inside the diaphragm walls provide lateral wall deflections during the process of excavation for construction control. In addition, the inclinometer readings can also be used to derive the wall curvatures and hence the bending moments along the wall section. By fitting a high order polynomial function to the inclinometer readings, the corresponding wall curvatures can be obtained by taking the second derivative of the polynomial function.

PERFORMANCE OF THREE INSTRUMENTED PANELS

This section describes the performance of three instrumented panels at the Esplanade Car Park. The locations of the three sets of instrumented wall panels, namely panel P3, P19, and P50 are shown in Fig. 1. Results from both the inclinometer and strain gauges installed within the same wall panel are presented and discussed herein. Details of the wall panel dimensions and the locations of the strain gauges are shown in Table 1. Reduced level (RL) is taken as mean sea level plus 100m. The spot-weldable vibrating wire strain gauges were installed on steel reinforcement on both faces of the diaphragm walls. The inclinometer and strain gauges were installed along the same cross section of the wall. Initial readings for both the wall inclinometer and strain gauges were taken at the same time before the excavation began. Subsequent readings at the different phases of the excavation were also taken at the same time.

These instrumentation results are used to compare the bending moments deduced from wall inclinometer and strain gauge readings. The inclinometer readings were fitted with a seventh-degree polynomial, and the double differentiation of this polynomial gave the wall curvatures. The coefficient of determination r2 values, obtained during the curve fitting ranged from 0.9963 to 0.9997, indicating minimal error during the process of curve fitting. Details of deducing wall bending moments from wall inclinometer readings for an uncracked and cracked wall section have been reported by Poh et al. (1997), and hence are not repeated herein. The steel strains obtained from the pairs of strain gauges were also used to compute the wall curvatures.

Case 1: Panel 3

A total of twelve pairs of vibrating wire strain gauges and a wall inclinometer ID1 were installed inside the wall during the construction of the wall panel P3. The ground water level across the site generally ranged from RL 101 to 102m. There was no water standpipe installed adjacent to this instrumented panel. The subsurface conditions adjacent to this panel are shown in Fig. 2, alongside the measured lateral wall deflections profiles for three stages of excavation at RL 102, 97, and 92m. The wall movement of the top of the wall during the second stage of excavation could be due to the openings in the slabs adjacent to this panel. Another possible explanation could be the large basement width; consequently it may have taken some time to complete the construction of the entire floor slab before its full stiffness could be achieved. The bending moments deduced from the wall inclinometer readings and the strain gauge readings, for the excavation at RL 102, 97, and 92m are shown in Figs. 3a, 3b, and 3c, respectively. Both the bending moments deduced from the wall inclinometer readings and the strain gauge readings take into account the effects of cracking of the diaphragm walls. These figures show that the bending moments deduced from the wall inclinometer readings for the three stages of excavation generally agree well with those deduced from the strain gauges readings. As it was a very large site, the construction works were carried out in smaller zones. Each construction stage shown in the figures represented a stage where approximately half the zones from the wall boundary were completed. The large reversal of bending moments shown in Figure 3(a) might have been due to presence of a completed slab near the boundary while excavation works still proceeded toward the inner zones. Figure 3(c) shows that for large part of the wall section, the deduced bending moments exceeded the cracking moments of the wall but were still within its 0.2mm crack width serviceability limit of 1350kNm.

Case 2: Panel 19

The instruments in wall panel P19 consisted of the wall inclinometer ID5 and eleven pairs of vibrating wire strain gauges. The ground water level was at RL 101m. The subsurface conditions adjacent to this panel are shown in Fig. 4, alongside the measured lateral wall deflections profiles for two stages of excavation at RL 97 and 92m. The bending moments deduced from the wall inclinometer readings and the strain gauge readings for the excavation at RL 97 and 92m are shown in Figs. 5a and 5b, respectively. These figures also show that the bending moments deduced from the wall inclinometer readings generally agree well with those deduced from the strain gauge readings.

Table 1 Wall panel dimensions and strain gauge locations

	Panel 3	Panel 10	Panel 50
Ground surface RL (m)	102.5	103.0	103.6
Wall panel thickness (m)	1.0	1.0	1.0
Wall panel width (m)	6.7	6.7	6.7
Wall panel depth (m)	35.5	30.0	23.0
RL Location of strain gauges RL (m)	72,76,80,84,87,90 92,94,96,98,100,102	72.9,77,81,85,88,91 93,95,97,99,101	83,87,90,92,94 96,98,100

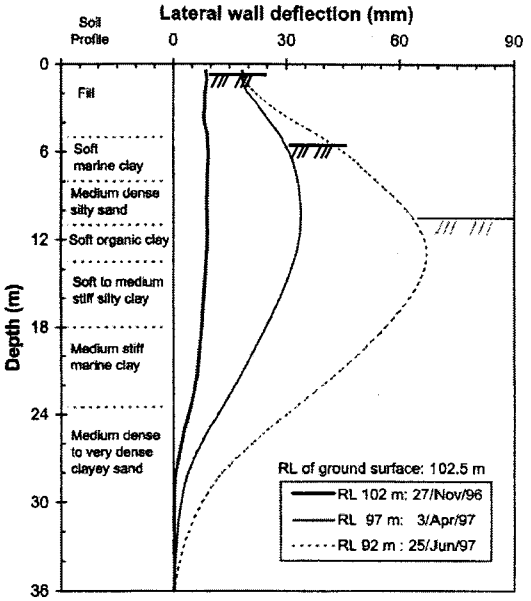

Fig. 2 Measured lateral wall deflections for three stages of excavation (Panel 3)

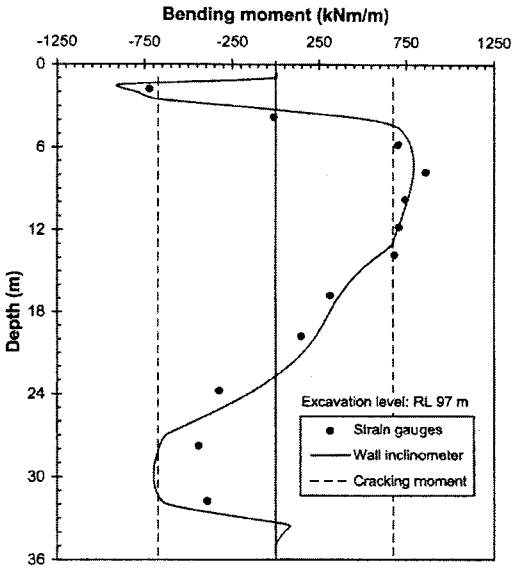

Fig. 3 Deduced wall bending moments for Panel 3: (b) at RL 97m

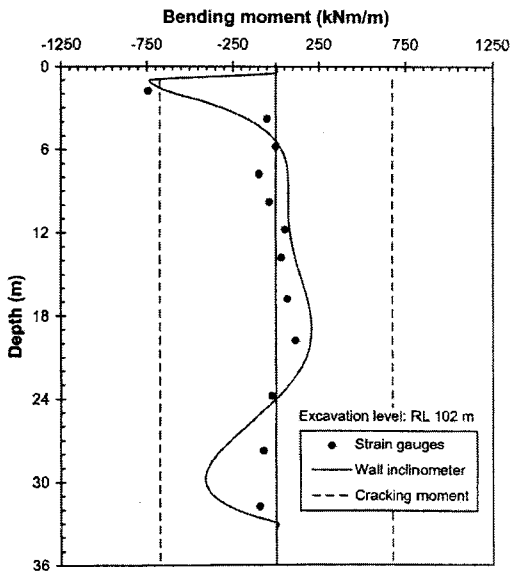

Fig. 3 Deduced wall bending moments for Panel 3: (a) at RL 102m

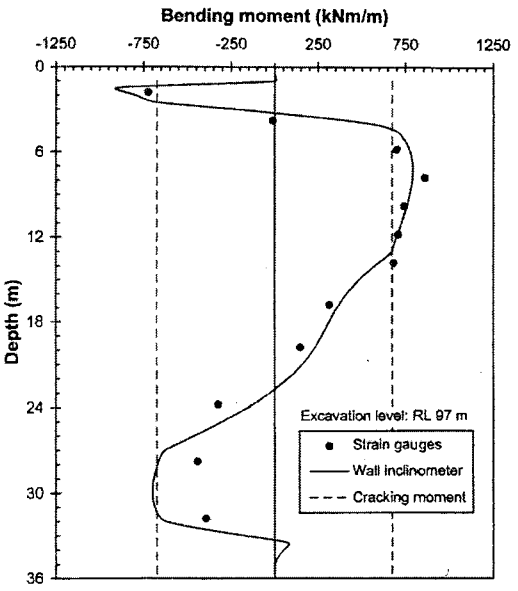

Fig. 3 Deduced wall bending moments for Panel 3: (c) at RL 92m

Case 3: Panel 50

The wall panel P50 consisted of eight pairs of vibrating strain gauges, and a wall inclinometer ID10. The ground conditions adjacent to this panel are shown in Fig. 6, alongside the measured lateral wall deflections for three stages of excavation at RL 99.2, 97.15, and 92m. The shape of these wall deflections differed from that reported for Case 1 and Case 2, with a large cantilever wall movement during the first stage of excavation. This trend was due to the deep cantilever excavation of 4.4m before the top slab was cast, combined with the low undrained shear strength of the soft soils and the relatively thinner layer of soft soils overlying the clayey sand layer. Similar observations have also been reported at other sites by Wong et al. (1996).

The bending moments deduced from the wall inclinometer readings and the strain gauge readings for excavation at RL 99.2, 97.15, and 92m are shown in Figs. 7a, 7b, and 7c, respectively. As with Case 1 and Case 2, these figures show that the bending moments deduced from the wall inclinometer readings generally agree quite well with those deduced from the strain gauge readings.

The results from these three cases, as well as previously reported studies by Poh et al. (1997) suggest that wall inclinometer readings provide an alternative method of measuring wall bending moments and the results are comparable with those obtained from strain gauge readings. Further instrumented case studies are required to confirm these findings

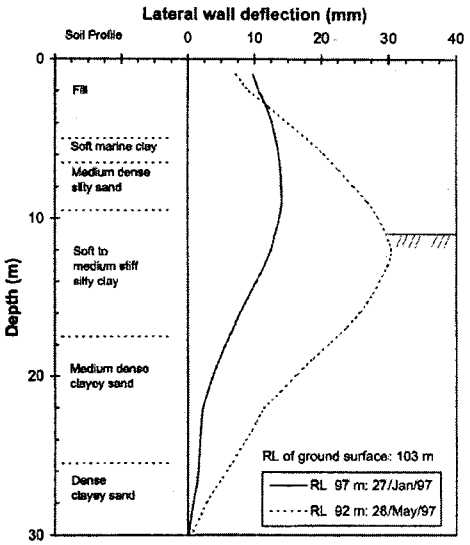

Fig. 4 Measured lateral wall deflections for two stages of excavation (Panel 19)

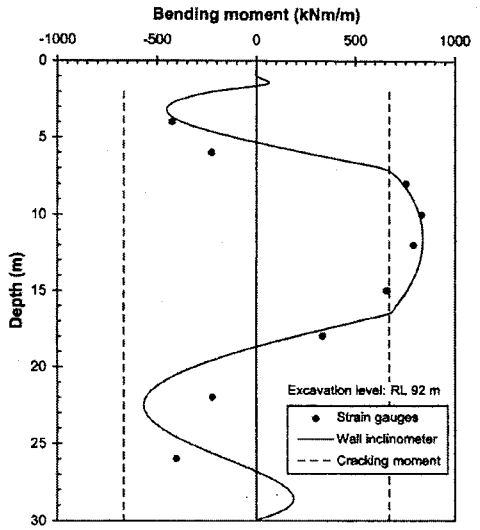

Fig. 5 Deduced wall bending moments for Panel 19: (b) at RL 92m

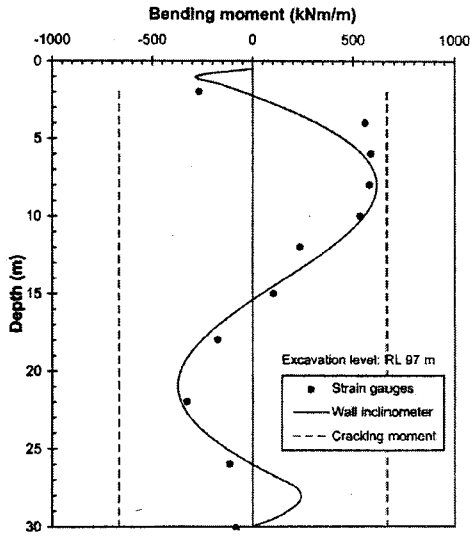

Fig. 5 Deduced wall bending moments for Panel 19: (a) at RL 97m

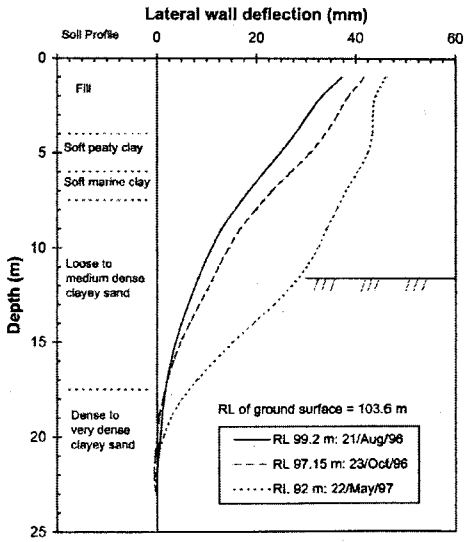

Fig. 6 Measured lateral wall deflections for three stages of excavation (Panel 50)

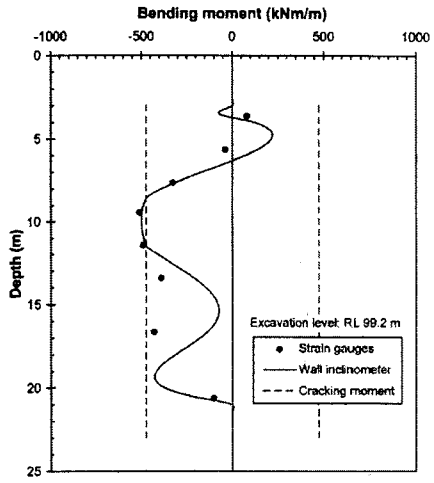

Fig. 7 Deduced wall bending moments for Panel 50: (a) at RL 99.2m

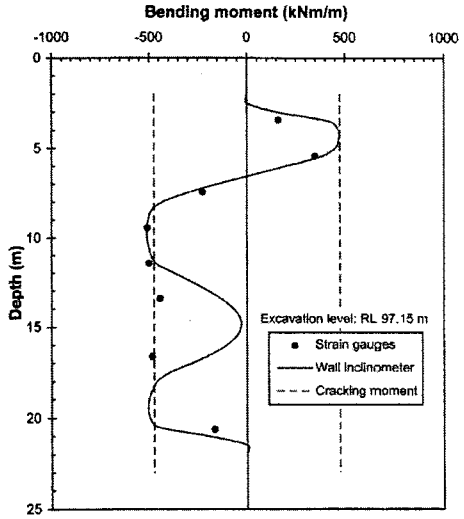

Fig. 7 Deduced wall bending moments for Panel 50: (b) at RL 97.15m

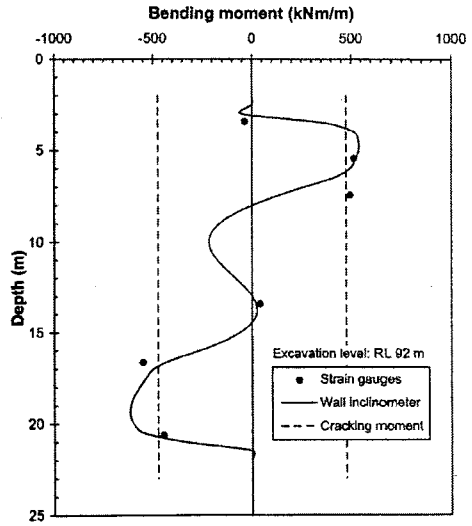

Fig. 7 Deduced wall bending moments for Panel 50: (c) at RL 92m

POST CONSTRUCTION RE-ANALYSIS OF WALL PANEL P3

Post construction re-analysis of the basement excavation was carried out for the section next to instrumented wall panel P3. The panel which was located at the south wall boundary of the site was selected because of the presence of a thick layer of soft soil in this locality. The combined thickness of the soft soil layers is approximately 15m. In addition, there were nine total lateral earth pressure cells installed in this section. The excavation was 10.5m deep and was retained by a 1.0m thick, 35.5m long diaphragm wall, with three levels of slabs as props. As indicated previously, the width of the wall panel was 6.7m. The top slab, mid-basement slab B1, and the base slab are at RL 102.2, 97.65, and 93.55m with a thickness of 0.2, 0.5, and 0.8m, respectively.

Ground Conditions

The subsurface conditions next to this wall section consisted of fill overlying soft soil layers that in turn was underlain by a medium dense to very dense clayey sand. A cross section of the soil profile is shown in Fig. 8. The fill layer was a 5m thick loose to medium dense silty sand fill, with standard penetration test (SPT) N values ranging from 5 to 18. Directly beneath the fill was a 3m thick layer of soft marine clay, followed by a 3m thick medium dense silty sand, a 2.5m thick soft organic clay, a 4.5m thick soft to medium stiff silty clay, and a 5.5m thick medium stiff marine clay. The untrained shear strength of the soft clay layers including the upper and lower marine clay layers shown in Fig. 8 were obtained from field vane shear tests. The medium stiff marine clay was in turn underlain by a medium dense to very dense clayey sand layer. The SPT N value of this medium dense to very dense clayey sand layer increased with depth, with N = 11 at the top of the layer and N = 115 at a depth of 38 m below the ground surface. The medium dense to very dense clayey sand layer belongs to the Old Alluvium Formation (Public Works Department 1976)

Construction Sequences

The construction sequence adjacent to the instrumented panel P3 was as follows:

1) Construction of a 1.0m thick, 35.5m deep diaphragm wall (May 24, 1996)
2) Excavation to RL 102m (stage 1; November 27, 1996)
3) Construction of the top slab at RL 102.3m (stage 2; early December, 1996)
4) Excavation to RL 97m (stage 3; April 3, 1997)
5) Construction of B1 slab at RL 97.65m (stage 4; mid April 1997)
6) Excavation to RL 92m (stage 5; June 25, 1997)
7) Construction of the base slab at RL 93.55m (stage 6; end of July, 1997)

As the basement excavation plan area was very large, the main construction activities, namely the excavation of the subsoil and the construction of the slabs, were subdivided into zones, with plan area of approximately 30 to 40 m by 30 to 40m.

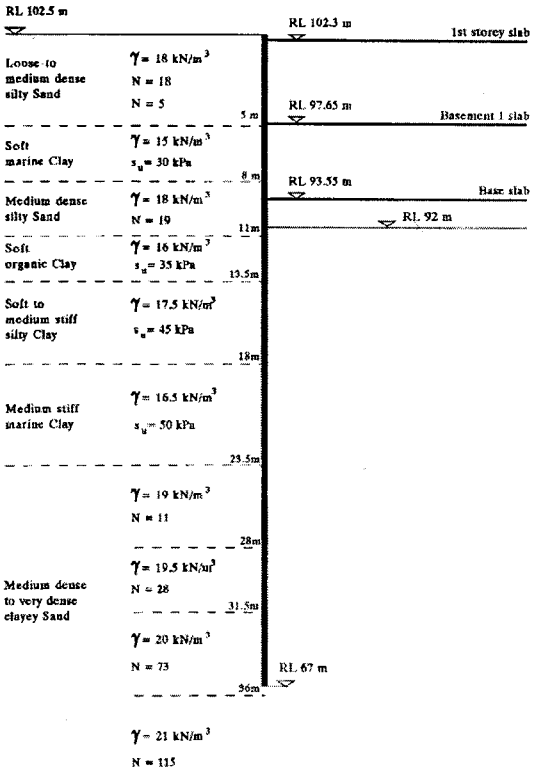

Fig. 8 Cross section and soil profile for Panel 3

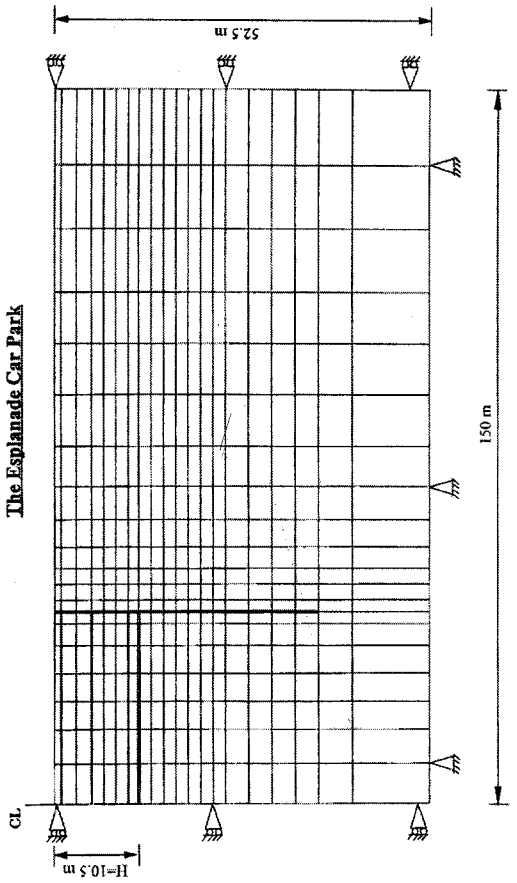

Fig. 9 Finite element mesh

Instrumentation and Monitoring Program

As mentioned previously, the monitoring instruments consisted of a single wall inclinometer, twelve pairs of vibrating wire strain gauges installed on the steel reinforcement, and nine jack-out total earth pressure cells. They were installed inside the wall during the construction of the wall panel. The total earth pressure cells were located at RL 97, 91, 87, 82, and 72m.

The pressure cells were installed in pairs, with one on each side of the wall except at RL 97 where there was only one pressure cell installed on the soil face-. The tip of the wall inclinometer was located at the same depth as the toe of the wall.

Finite Element Program Used in Analysis

A modified version of the finite element program EXCAV was used in the post construction re-analyses. This program has been widely used and tested by a number of researchers such as Duncan and Chang (1977), Broms et al. (1986), Wong and Broms (1989), and Wong et al. (1996). The program can be used to simulate excavations in clay and sand under plane strain conditions. Four-node isoparametric elements are used to model the soil medium. The walls and slabs have been modeled by structural beam elements. The program uses the hyperbolic model (Duncan et al. 1980) to simulate the nonlinear, stress-dependent, and inelastic behavior of the soils. The nonlinear stress-strain behavior of the soil is modeled using a small linear incremental procedure with small loading or unloading steps.

The program can simulate the sequential nature of the excavation and strut installation. An increment of analysis may consist of excavation of a layer of soil and application of loads. During any increment of the analysis, structural elements such as struts may be inserted in the analysis. The program can simulate the effects of the cracking of diaphragm walls by using a beam element with a composite moment-curvature curve, consisting of a straight line followed by a hyperbolic curve, to define the corresponding moment-curvature relationship for the diaphragm walls. For the post construction re-analysis, the moment-curvature relationship of the diaphragm wall is derived based on Branson's (1977) formula as outlined in Poh et al. (1997).

The same program was used previously by Poh et al. (1997) to back-analyze the performance of two instrumented case histories involving propped excavations supported by diaphragm walls in stiff residual soils. The analyses also incorporated the effects of concrete cracking of the diaphragm wall and the results of analysis agreed well with the measured values.

Soil Parameters Used in Analysis

For many routine excavation projects, as was the case for this project, many of the required soil properties needed for the finite element analysis are lacking. Consequently, the soil properties used in finite element analysis were estimated using the procedure outlined below. The same procedure was used for other projects in Singapore (Wong et al. 1996; Poh et at. 1997).

From the results of the site investigation, the relationship between undrained shear strength s_u and depth

can be established. For clays, the over consolidation ratio (OCR) profile can be back-calculated from the simplified relationship OCR = (B/a)1.25 from Ladd et al. (1977) and an assumed Su/σv' value of 0.25 and 0.3 for normally consolidated clay for soft and stiff soils, respectively, where *B* and *a* are the normalized undrained shear strength of an overconsolidated clay and a normally consolidated clay, respectively.

The coefficient of earth pressure at rest can be calculated by using the relationship Ko=(1-Sinϕ')OCRSinϕ' from Mayne and Kulhawy (1982), where ϕ' is the effective friction angle of the soil. The coefficient of lateral earth pressure K that is used in the analysis is calculated from the relationship K=(σ'h+u)/(σ'v+u) in which σ'h=Koσ'v u is the pore water pressure, σ'v is the vertical effective overburden stress, and σ'h is the horizontal effective overburden stress.

The undrained Young's modulus is obtained from the relationship between the undrained soil modulus, the undrained shear strength, the plasticity index, and the overconsolidation ratio proposed by Duncan and Buchignani (1976). Based on this relationship, the undrained secant soil modulus (E_u) is calculated by using $E_u = M_m.s_u$ in which M_m, the modulus multiplier, is a function of the computed OCR profile and the plasticity index. The initial tangent modulus E_i that is used in the finite element analysis is taken to be twice the undrained secant modulus E_u. The short-term undrained analysis is carried out using a total stress analysis approach. The clay deposits are assumed to be saturated and incompressible with a Poisson's ratio of 0.49. The drained modulus of the soil layer was obtained by assuming the shear modulus of the soil remain unchanged.

Finite Element Analysis

The excavation was analyzed under undrained and plane strain conditions based on total stress. The analysis modeled a half width of the excavation where the left-hand boundary of the mesh represents the line of symmetry at the center line of the excavation. The finite element mesh is 150m long, 52.5m deep, and consists of 400 elements and 441 nodes, and is shown in Fig. 9 together with the assumed boundary conditions.

No interface elements were used to model the wall-soil interface. The soil properties used in the analysis are shown in Table 2. A grade G40 concrete, with cube compressive strength f_{cu} of 40MPa (equivalent to a cylinder compressive strength f_c' of 32MPa, assuming $f_c' = 0.8\, f_{cu}$) was used for the diaphragm wall panel. The compression and tension steel content of the wall panel was 0.38 and 0.76% of the gross area of the wall section, respectively. The gross cover thickness of the wall (inclusive of a 30mm sacrificial cover) was 75mm and the moment of inertia of the wall of 8.14 x 10-2m4 was adopted in the analysis. Based on BS 8110 (BSI 1985), the modulus of concrete was taken as 28 GPa.

In the analysis, the walls and slabs were modeled as beam elements. The effects of construction of the diaphragm wall are not considered. The analysis takes into account of the effects of cracking of the diaphragm wall by using a composite curve consisting of a linear line followed by a hyperbolic curve to define the moment-curvature relationships for the beam sections. The moment-curvature relationships for the diaphragm walls are based on Branson's (1977) formula.

The moment-curvature relationships calculated based on Branson's (1977) formula, and that used in the finite element analysis are shown in Fig. 10. This figure shows that the concrete cracking reduces the wall bending moment significantly. Fig. 10 shows that after cracking is initiated, the continued use of an uncracked section in the analysis would over-predict the wall bending moments, especially when the magnitude of the wall curvature is large. However, the use of a fully cracked section with the concrete in tension ignored would under-predict the wall bending moments.

Table 2 Soil properties used in the finite element analysis

Soil Layer (m)	γ (kN/m^3)	E_i (kPa)	R_f	μ	s_u (kPa)	Φ (°)	K
0 - 3.0	18.0	51300	0.70	0.35	0	35	0.76
3.0 - 5.0	17.5	23400	0.70	0.35	0	30	0.74
5.0 - 8.0	15.0	18000	0.75	0.49	30	0	0.84
8.0 - 11.0	18.0	54100	0.70	0.35	0	35	0.77
11.0 - 13.5	16.0	20100	0.75	0.49	35	0	0.82
13.5 - 18.0	17.5	28300	0.75	0.49	45	0	0.80
18.0 - 23.5	16.5	30000	0.75	0.49	50	0	0.82
23.5 - 28.0	19.0	46200	0.70	0.35	0	35	0.73
28.0 - 31.5	19.5	96600	0.70	0.35	0	35	0.84
31.5 - 36.0	20.0	241000	0.70	0.35	0	38	0.98
> 36.0	21.0	310000	0.70	0.35	0	38	1.03

Results of Finite Element Analysis

The measured and the computed lateral wall deflections for the three stages of excavation at RL 102, 97, and 92m are shown in Fig. 11. Generally, the computed lateral wall deflections agree reasonably well with the measured values, in both the shape and magnitude of the deflection curves. For the first stage of excavation at RL 102m, the computed lateral wall movements are slightly smaller than the observed values.

For the second and third stages of excavation at RL 97 and 92m, respectively, the computed maximum lateral wall movements are larger than the corresponding observed values, with their locations shifted slightly downwards. In addition, the computed movements at the top of the wall are much smaller as compared to the observed values. As mentioned previously, during the second stage of the excavation, as shown in Fig. 11, the measured values indicated that there was considerable movement observed at the top of the wall. This trend may be due to the presence of large openings in the slabs adjacent to this panel. Another possible reason could be due to the large basement width; consequently, it may have taken some time to complete the construction of the entire floor slab before its full stiffness could be achieved. Fig. 11 also shows that the computed wall toe movements are larger than the measured values. This trend has been commonly reported for the back-analysis of propped excavations, and may possibly be due to the small strain behavior of the medium dense to very dense clayey sand layer near to the toe of the wall.

The bending moments deduced from the wall inclinometer and strain gauge readings as well as the computed values corresponding to the excavation level at RL 102, 97, and 92m are shown in Figs. 12a, 12b, and 12c, respectively. Figs. 12a and 12b show that the computed wall bending moments generally agree quite well with the deduced values except for the top portion of the wall, where the computed bending moments could not predict the reversal of the bending moments. Fig. 11 shows that the computed lateral wall deflections near the top portion of the wall differ from the measured values, in both shape and magnitude. This may explain why the computed bending moments for this portion of wall differ from the measured values. Fig. 12c shows that the computed wall bending moments for the excavation at RL 92m agree reasonably well with those deduced from the wall inclinometer and strain gauge readings, in both the shape and magnitude. Generally, the computed values are slightly larger than the corresponding measured values.

The total lateral earth pressures monitored using vibrating wire total lateral earth pressures (manufactured by Slope Indicator) during the three stages of excavation for both the measured and computed values are shown in Fig. 13. This figure shows that the computed total lateral earth pressures decrease during the progress of the excavation, except for the top 6m of the soil behind the wall (the active side) where there was an increase in total lateral earth pressures behind the wall during excavation, as the top of the wall was pushed backward slightly. The measured values also show a similar trend of reduction in total lateral pressures during excavation. Similar trends of reduction in total lateral earth pressures on the active and passive sides of the wall with excavation depth for excavations in soft clays have also been reported by other researchers such as Dibiagio and Roti (1972), Karlsrud (1983), Tamano et al. (1996a), and Tamano et al. (1996b). By comparing the observed values for the three pairs of total earth pressure cells directly below the bottom of the excavation, at a depth of 11.5, 15.5, and 20.5m, Fig. 13 shows that the reduction in the total lateral earth pressures at the front side of the wall (passive side) occurred at a much faster rate than the corresponding values for those behind the wall. This trend may be due to the removal of overburden pressure directly above these pressure cells. Excavations in soft clay reported by Karlsrud (1983) also showed a similar trend.

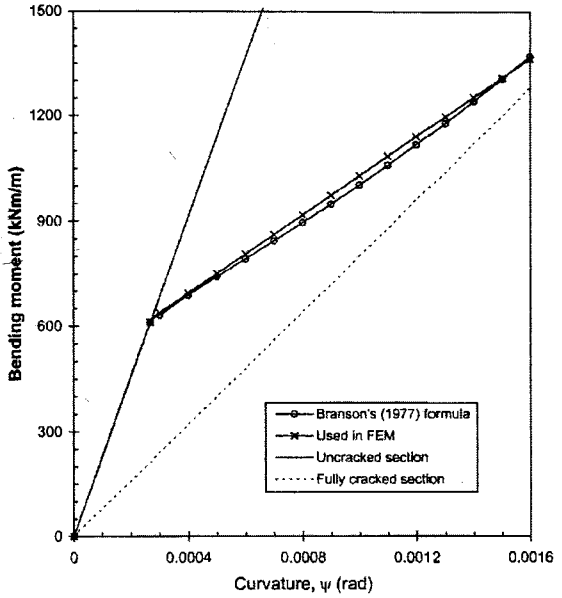

Fig. 10 Moment-curvature relationship

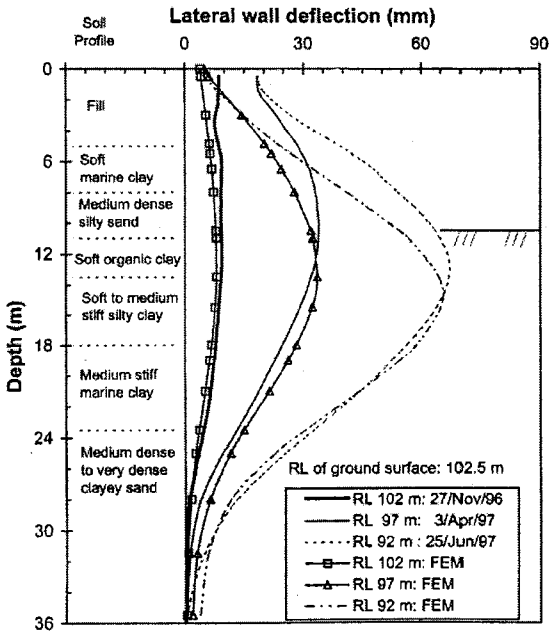

Fig. 11 Measured and computed wall deflections for Panel 3

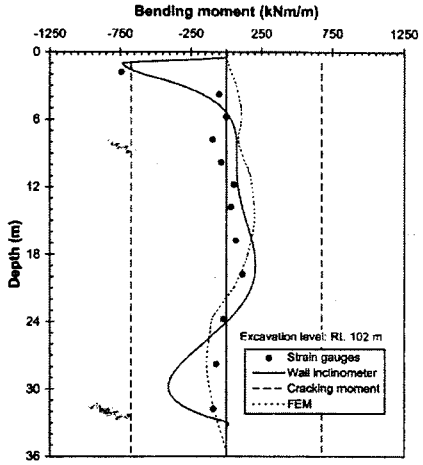

(a)

Fig. 12 Deduced and computed wall bending moments for Panel 3: (a) at RL 102m

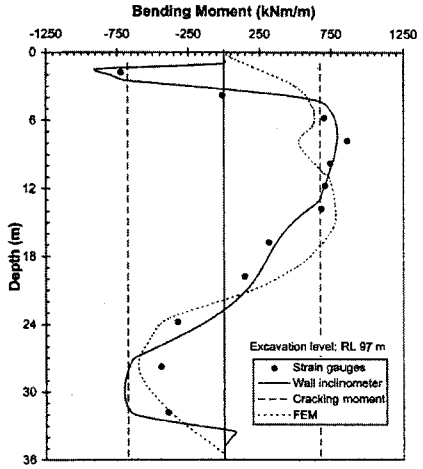

(b)

Fig. 12 Deduced and computed wall bending moments for Panel 3: (b) at RL 97m

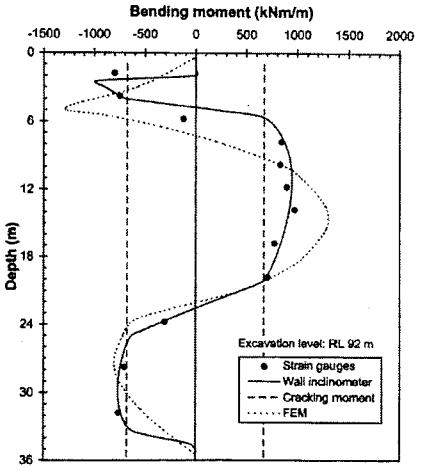

(c)

Fig. 12 Deduced and computed wall bending moments for Panel 3: (c) at RL 92m

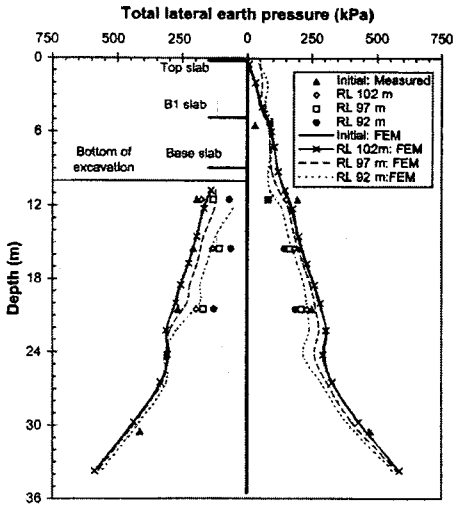

Fig. 13 Observed and computed total lateral earth pressures (Panel 3)

Effects of Concrete Cracking

The structural design of diaphragm wall in Singapore is based on limit state design, where calculations are carried out at the failure state (ultimate limit state) for loads larger than those expected in service (factored loads), and checks are made of the deflections and cracking at service load levels (serviceability limit state). The ultimate limit state is generally based on BS 8110 (BSI 1985). Besides serving as soil retaining structures, diaphragm walls are also frequently designed based on requirements for water retaining structures. Hence, the serviceability limit state has to adhere to BS 8007 (BSI 1987), which is generally based on a design crack width of 0.2mm. In other words, the effects of concrete cracking are incorporated in the structural design of diaphragm walls in Singapore. The bending moments used in the structural design of diaphragm walls are generally obtained from numerical analysis such as one- and two-dimensional finite element methods. Currently, many finite element analyses are carried out assuming that the wall behaves linear elastically and that the wall is assumed to be uncracked. Where reductions in the flexural stiffness are simulated, such reductions are predetermined by the engineer performing the analyses and inputted into the analyses.

This section highlights the differences in the behavior of the diaphragm wall when the wall is assumed to behave linear elastically, and when the effects of wall cracking are incorporated in the finite element analysis. In the former, the finite element analysis was carried out by modeling the wall with linear elastic beam elements, with the other parameters remaining unchanged.

The results for the excavation at RL 92m, with and without considering the effects of concrete cracking on the lateral wall deflections and wall bending moments are shown in Figs. 14 and 15, respectively. Fig. 14 shows that the concrete cracking results in larger (15%) lateral deflections of the 1.0m thick wall compared with the linear elastic analysis. The maximum lateral wall deflection for the analysis incorporating the effects of cracking was 65.0mm, compared with 56.5mm for the linear elastic analysis.

Poh et al. (1997) have shown that for excavations in stiff soils supported by 0.6m walls, cracking was accompanied by a smaller increase (6%) in lateral wall deflection. This trend may be because the cracking is larger for the Esplanade Car Park.

Fig. 15 shows that the computed wall bending moments for the analysis assuming the wall behaves linear elastically are as much as 60% higher than those for the analysis that incorporated the effects of concrete cracking. This is likely to be due to the large wall curvatures developed during excavation.

As Ng et al. (1992) have pointed out, both the selection of the appropriate concrete cracking and the evaluation of realistic concrete parameters that account for creep and shrinkage can significant influence the computed bending moments. To reduce uncertainty in the computed bending moments, they recommended taking and testing concrete cores from the wall close to the time of interest, rather than rely on typical concrete modulus values taken from BS8110.

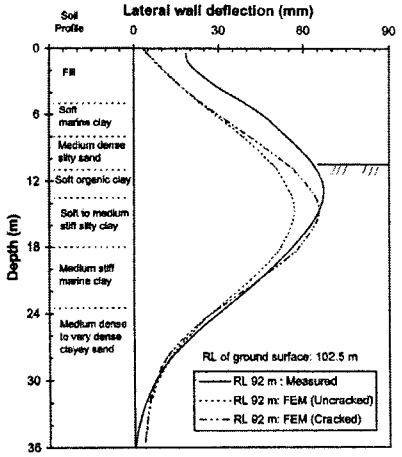

Fig. 14 Effects of cracking on lateral wall deflections for excavation to RL 92m

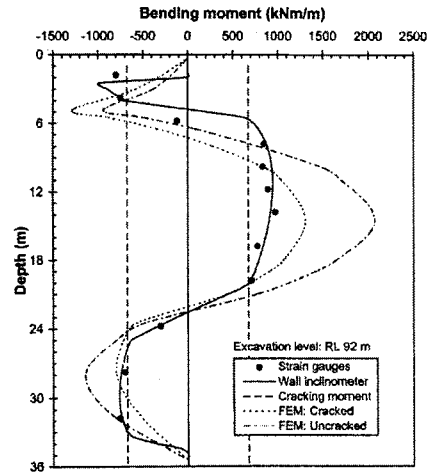

Fig. 15 Effects of cracking on wall bending moments for excavation to RL 92m

SUMMARY AND CONCLUSIONS

The following summary and conclusions are made:

Two methods of deducing bending moments in diaphragm walls were used in this project. The first method involves deducing bending moments from strain gauge readings while the second method is from wall deflection readings. Bending moments deduced from three instrumented wall panels where there were wall inclinometer and strain gauges installed in the same panel have been presented. The results show that the bending moments deduced from wall inclinometer readings agree well with those obtained from strain gauge readings. These results suggest that wall inclinometers, commonly available for most excavation projects, are an inexpensive alternative for deducing bending moments in diaphragm walls.

Post construction re-analyses were carried out using a finite element program that incorporated the effects of cracking of the wall. The computed results agreed well with the observed values. Results of analysis indicate that cracking is accompanied by a substantial reduction in the bending moments in the diaphragm wall.
Hence, the use of linear elastic wall properties in the finite element analysis would significantly over-predict the wall bending moments especially for cases associated with large wall curvatures. The study also indicates that the use of a linear elastic or an uncracked wall properties results in smaller lateral wall movements as compared to an analysis that incorporated the effects of concrete cracking.

ACKNOWLEDGEMENTS

The results presented in this paper are part of the research collaboration between the former Public Works Department of Singapore and the School of Civil and Environmental Engineering, Nanyang Technological University

REFERENCES

AMERICAN CONCRETE INSTITUTE. (1992). Building code requirements for reinforced concrete (ACI 318/318R-89). American Concrete Institute, Detroit, Michigan.

BRANSON, D.E. (1977). *Deformation of concrete structures.* McGraw-Hill, New York, N.Y.

BRITISH STANDARDS INSTITUTION. (1985). British standard: Structural use of concrete: Part 1. Code of practice for design and construction. BSI, BS 8110. London, England.

BRITISH STANDARDS INSTITUTION. (1987). British standard code of practice for design of concrete structures for retaining aqueous liquids. BSI, BS 8007. London, England.

BROMS, B.B., WONG, I.H. and WONG, K.S. (1986). Experience with finite element analysis of braced excavation in Singapore. *Proceedings of the 2nd International Symposium on Numerical Models in Geomechanics*, A. A. Balkema, Rotterdam, Netherlands, pp. 309-324.

DIBIAGIO, E. and ROTI, J.A. (1972). Earth pressure measurements on a braced slurry-trench wall in soft clay. *Proceedings of the 5th European Conference on Soil Mechanics and Foundation Engineering*, Spanish Society for Soil Mechanics and Foundations, Madrid, Spain, 1, pp. 473-483.

DUNCAN, J.M. and BUCHIGNANI, A.L. (1976). An engineering manual for settlement studies. Geotechnical Engineering Report, Department of Civil Engineering, University of California, Berkeley, California, U. S. A..

DUNCAN, J.M., BYRNE, P., WONG, K.S. and MABRY, P. (1980). Strength, stress-strain and bulk modulus parameters for finite element analysis of stresses and movements in soil masses. Geotechnical Engineering Research Report No. VCB/GT/80-81, University of California, Berkeley, California, U. S. A.

DUNCAN, J.M. and CHANG, C.S. (1977). EXCAV: A computer program for analysis of stresses and movements in excavations. Geotechnical Engineering Research Report No. TE 77-4, University of California, Berkeley, California, U. S. A.

GHALI, A. (1993). Deflection of reinforced concrete members: A critical review. *ACI Structural Journal*, Vol. 90, No. 4, pp. 364-373.

KARLSRUD, K. (1983). Performance and design of slurry walls in soft clay. *Norwegian Geotechnical Institute*, Oslo, Norway, Vol. 149, pp. 1-9.

KONG, F.K. and EVANS, R.H. (1987). *Reinforced and prestressed concrete*. 3rd ed., Van Nostrand Reinhold, London, England.

LADD, C.C., FOOTE, R., ISHIHARA, K., SCHLOSSER, F. and POULOS, H.G. (1977). Stress-deformation and strength characteristics. *Proceedings of the 9th International Conference on Soil Mechanics and Foundation Engineering*, State-of-the-art-report, Tokyo, Japan, Vol. 2, pp. 421-494.

MACGREGOR, J.G. (1997). *Reinforced concrete: Mechanics and design*. 3rd. ed., Prentice Hall, New Jersey.

MAYNE, P.W. and KULHAWY, F.H. (1982). Ko-OCR relationships in soil. *ASCE Journal Geotechnical Engineering*. Vol. 108, No. 6, pp. 851-872.

NG, C.W.W., LINGS, M.L. and NASH, D.F.T. (1992). Back-analysis the bending moment in a concrete diaphragm wall. *The Structural Engineer*, Vol. 70, No. 23 and 24, pp. 421- 426

POH, T.Y., WONG, I.H. and CHANDRASEKARAN, B. (1997). Performance of two propped diaphragm walls in stiff residual soils. *ASCE Journal Performance of Constructed Facilities*. Vol. 11, No. 4, pp. 190-199.

PUBLIC WORKS DEPARTMENT. (1976). Geology of the Republic of Singapore.

TAMANO, T., FUKUI, S., MIZUTANI, S., TSUBOI, H. and HISATAKE, M. (1996). Earth and water pressures acting on the excavation side of a braced wall in soft ground. *Proceedings of the International Symposium on Geotechnical Aspects of Underground Construction in Soft Ground*, A. A. Balkema, Rotterdam, Netherlands, pp. 207-212.

TAMANO, T., FUKUI, S., SUZUKI, H. and UESHITA, K. (1996). Stability of slurry trench excavation in soft clay. *Soils and Foundations*, Japanese Geotechnical Society, Tokyo, Japan, Vol. 36, No. 2, pp. 101-110.

WONG, I.H., POH, T.Y. and CHUAH, H.L. (1996). Analysis of case histories from the construction of the Central Expressway in Singapore. *Canadian Geotechnical Journal*, Ottawa, Canada, Vol. 33, No. 5, pp. 732-746.

WONG, K.S. and BROMS, B.B. (1989). Lateral wall deflections of braced excavations in clay. *ASCE Journal Geotechnical Engineering*. Vol. 115, No. 6, pp. 853-870